Integrated Aerodynamic Load/Dynamic Optimization of Helicopter Rotor Blades

Aditi Chattopadhyay*
Analytical Services & Materials, Inc., Hampton, Virginia 23666
Joanne L. Walsh†
NASA Langley Research Center, Hampton, Virginia 23665
and
Michael F. Riley‡
Lockheed Engineering and Management Services Company, Inc., Hampton, Virginia 23666

An integrated aerodynamic load/dynamic optimization procedure is used to minimize blade weight and 4 per rev vertical hub shear for a rotor blade in forward flight. Through the coupling of aerodynamic loads and dynamics into the optimization procedure, the effects of changes in air loads due to changes in the design variables are incorporated. Both single and multiple objective functions are used in the optimization formulation. The "Global Criteria Approach" is used to formulate the multiple objective optimization, and results are compared with those obtained by using single objective function formulations. Constraints are imposed on natural frequencies, autorotational inertia, and centrifugal stress. The program CAMRAD (Comprehensive Analytical Model of Rotorcraft Aerodynamics and Dynamics) is used for the blade aerodynamic and dynamic analyses, and the program CONMIN is used for optimization. The vertical air load distributions on the blade, before and after optimization, are compared. The total power required by the rotor to produce the same amount of thrust per area is also calculated before and after optimization. Results of this study indicate that integrated optimization can significantly reduce the blade weight and vertical hub shear as well as oscillatory vertical blade air load distributions and the total power required.

Nomenclature

A = blade cross-sectional area, ft^2
A_i = cross-sectional area of ith segment, ft^2
AI = autorotational inertia, lb-ft^2
c = chord, ft
C_P = power coefficient
C_T = thrust coefficient
E = Young's modulus, lb/ft^2
EI_{xx}, EI_{zz} = bending stiffnesses, lb-ft^2
f_3, f_4, f_5, f_6 = natural frequencies of first four coupled elastic modes, per/rev
$F, \hat{F}$ = objective functions
FS = factor of safety
F_p = blade vertical air load, lb/ft
F_z = amplitude of 4/rev vertical hub shear, lb
g_j = jth constraint function
GJ = torsional stiffness, lb-ft^2
I_{xx}, I_{zz} = principal area moments of inertia about reference axes, ft^4
k = principal radius of gyration, ft
k_{xx}, k_{zz} = radius of gyration about reference axes, ft
L_i = length of ith segment, ft
N = number of nodes
NCON = number of constraints
NDV = number of design variables
NSEG = number of blade segments
R = blade radius, ft
s = thrust-weighted solidity
w_j = nonstructural weight per unit length at the jth node, lb/ft
W = total blade weight, lb
W_i = weight of ith segment, lb
x, y, z = reference axes
$\hat{y}_i$ = distance from the root to the center of the ith segment, ft
Y = nondimensionalized radial distance
α = prescribed autorotational inertia, lb-ft^2
λ = taper ratio
ϕ_i = ith design variable
ρ_i = weight density of the ith segment, lb/ft^3
μ = advance ratio, ratio of aircraft speed to tip speed of rotor
σ_i = centrifugal stress in ith segment, lb/ft^2
σ_{max} = maximum allowable stress, lb/ft^2
Ψ = blade azimuth angle, deg
Ω = rotor speed, rad/s

Subscripts

L = lower bound
r = root value
t = tip value
U = upper bound

Presented as Paper 89-1269 at the AIAA/ASME/ASCE/AHS 30th Structures, Structural Dynamics, and Materials Conference, Mobile, AL, April 3–5, 1989; received Aug. 9, 1989; revision received April 2, 1990; accepted for publication April 20, 1990.

*Research Scientist; currently, Assistant Professor, Department of Aerospace and Mechanical Engineering, Arizona State University, Tempe, AZ 85287. Member AIAA.

†Aerospace Engineer, Interdisciplinary Research Office. Member AIAA.

‡Systems Analyst.

Introduction

IN recent years structural optimization has become a practical tool that can expedite mechanical design.[1-3] While this technique has received wide attention for fixed wing aircraft,[1]

it is less frequently used in the rotary wing industry.[4] In the past, the conventional helicopter rotor blade design process was controlled mainly by the designer's experience and by trial and error. Today, with improved understanding of helicopter analyses and efficient optimization schemes, attempts are being made to apply design optimization techniques and to reduce expensive man-in-the-loop iterations. References 5–9 have addressed some applications of optimization to rotorcraft. An important criterion in rotor blade design has been reduced vibration. For a helicopter in forward flight, the nonuniform flow passing through the rotor causes oscillating air loads on the rotor blades that are translated into undesirable vibratory shear forces and bending moments at the hub. In the conventional design process, vibration reduction has been accomplished by postdesign addition of lumped/tuning masses, which may cause significant increases in the blade weight. Hence an important design consideration is to obtain an optimum blade design for reduced vibration without incorporating a weight penalty.[10–18]

In most of the optimum helicopter rotor design work,[8,11–15] criteria related to a single discipline was addressed for each design problem. The blade design was treated as a series of nearly independent design tasks with little consideration of the couplings and interactions between disciplines. For example, only blade aerodynamic requirements were considered in Ref. 8. In Refs. 11 and 12, only dynamic design requirements were considered. Blade structural requirements only were considered in Ref. 13. In Refs. 14 and 15, minimum weight designs were determined for articulated rotor blades with rectangular and tapered planforms in the absence of air loads. The necessity of merging appropriate disciplines to obtain an integrated design procedure is being recognized. With improved understanding of helicopter analyses, it is now possible to include the couplings between the disciplines in the optimization procedure. Some initial investigations of partially integrating some of these disciplines are presented in Refs. 6 and 16–19. In Ref. 6 the dynamic and aeroelastic requirements were integrated and in Refs. 16–18 the dynamic design requirements were coupled with prescribed air loads in the analysis. Reference 19 presented a formulation of the integrated procedure involving dynamics and aerodynamics.

Currently at NASA Langley Research Center, there is an effort to integrate various disciplines in the rotor blade design process.[22] The present paper describes a part of this effort. The purpose of this work is to take an initial step in integrated optimum design of a rotor blade by coupling two important technical disciplines—blade aerodynamic loads analysis and dynamics. The aerodynamic loads analysis is included inside the optimization loop, and the blade air loads are updated as the design variables change during each step of the design optimization. A trim analysis is part of the procedure, and the blade is trimmed at each optimization cycle. Design variables affecting both disciplines are optimized based on a coupled aerodynamic and dynamic blade analysis. This paper addresses the design problem of reducing the blade weight and the 4 per rev (4/rev) vertical hub shear. When both the weight and the shear are simultaneously minimized, a multiple objective function technique is needed. A method known as the "Global Criteria Approach"[21] is used. The optimization procedure developed is applied to a blade test problem. Results obtained with a multiple objective function formulation are compared with two single objective function formulations—one with the blade weight as the objective function and the other with the 4/rev vertical hub shear as the objective function.

Problem Description

The design goal is to minimize the weight and the 4/rev vertical hub shear of a rotor blade in forward flight. Constraints are imposed on the first four coupled elastic flap-lag (rotating) natural frequencies to prevent them from falling into the critical ranges. These bounds are selected by careful consideration of the blade frequency vs rotor speed diagram and the associated frequency coalescence points. A prescribed lower bound on the blade autorotational inertia and an upper bound on the blade centrifugal stress are included as constraints.

As shown in Fig. 1, the blade has a linear taper along the blade planform. The blade taper ratio λ is given by

$$\lambda = c_r/c_t$$

where c_r is the root chord and c_t is the tip chord. The design variables are the following: EI_{xx_r}, EI_{zz_r}, GJ_r, λ, c_r, k_r, and w_j ($j=2,\ldots,N$). The lumped nonstructural weight at node 1 is not used as a design variable since it involves contribution from the hub.

Optimization Formulation

Three problem formulations are studied. The first formulation minimizes the blade weight W, the second minimizes the 4/rev vertical shear F_z, and the third minimizes the weight and the 4/rev shear simultaneously. In the latter, the Global Criteria Approach,[21] in which the optimum solution is obtained by minimizing a "global criterion" $F(\phi)$ is used, where

$$F(\phi) = \left[\frac{W(\phi) - W(\phi_1^*)}{W(\phi_1^*)}\right]^2 + \left[\frac{F_z(\phi) - F_z(\phi_2^*)}{F_z(\phi_2^*)}\right]^2 \qquad (1)$$

subject to

$$g_j(\phi) \le 0 \qquad j = 1,2,\ldots,\text{NCON}$$

The global criterion is thus defined as the sum of the squares of the relative deviations of the individual objective functions W and F_z from their respective individual optimum values. The design variable vector ϕ_1^* is obtained by minimizing the single objective function $W(\phi)$ subject to the set of constraints $g(\phi)$, and the design variable vector ϕ_2^* is obtained by minimizing F_z subject to the same constraints. Because of the highly nonlinear nature of the preceding function, the following objective function is used

$$\hat{F}(\phi) = \sqrt{F(\phi)}$$

where $F(\phi)$ is given by Eq. (1).

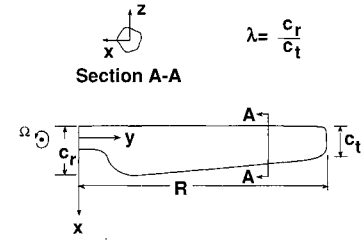

Fig. 1 Simplified rotor blade model with linear taper.

Table 1 Summary of the optimization problem

Formulation	1	2	3
Objective function	W	F_z	W and F_z
Constraints	$1 - f_k/f_{k_L} \le 0$		$k = 3,\ldots,6$
	$f_k/f_{k_U} - 1 \le 0$		
	$1 - AI/\alpha \le 0$		
	$FS\sigma_i/\sigma_{\max} - \le 0$		$(i = 1,\ldots,\text{NSEG})$
Design variables (see Fig. 1)	EI_{xx_r}, EI_{zz_r}, GJ_r, λ, c_r, r_r, w_j		$(j = 2,\ldots,N)$

The three formulations are summarized in Table 1, in which f_k represents the kth natural frequency where $k = 3, \ldots, 6$ (the first two modes are rigid-body modes). Frequencies f_3 through f_5 represent elastic flapping dominated modes, and f_6 is the first elastic lead-lag dominated mode.

Blade Analytical Representation

In this section, expressions for cross-sectional properties are presented for the blade model (Fig. 1) used in the optimization process. Since detailed design of the geometry of the blade cross section is not part of the current work, the cross-sectional area and the weight of the blade are formulated in terms of the design variables used. The total blade weight is comprised of the sum of the structural and the nonstructural weights of each of the spanwise blade segments. Since the nonstructural weights are the design variables specified at the nodes between segments in the sample problem, the segment nonstructural weight is calculated by averaging the weights at two associated nodes. The structural weight of the ith blade segment is $A_i \rho_i L_i$. Further details can be found in Ref. 26. The blade cross-sectional area is expressed in terms of the radii of gyration and the stiffnesses as follows:

$$A = (EI_{xx} + EI_{zz})/Ek^2 \tag{2}$$

where I_{xx} and I_{zz} are moments of inertia of the blade structural component about the z and x axes, respectively, and k is defined by

$$k^2 = k_{xx}^2 + k_{zz}^2 \tag{3}$$

and k_{xx} and k_{zz} are the radii of gyration associated with I_{xx} and I_{zz}, respectively.

The blade stiffnesses are contributed by the blade structural component only, and since the inertia $I \propto L^4$, it is assumed that the distribution of the stiffness EI_{xx} along the blade radius can be expressed in terms of its root value as follows

$$EI_{xx}(y) = EI_{xx_r}\left\{\frac{y}{R}\left[\frac{c(y)}{c_r} - 1\right] + 1\right\}^4 \tag{4}$$

where y is the blade radial location, and $c(y)$ is the chord distribution, which for a linear taper is given by

$$c(y) = c_r\left[\frac{y}{R}\left(\frac{1}{\lambda} - 1\right) + 1\right] \tag{5}$$

Similar expressions can be derived for $EI_{zz}(y)$ and $GJ(y)$.

The autorotational inertia AI of the blade is calculated from the segment weights as follows:

$$AI = \sum_{i=1}^{\text{NSEG}} W_i \hat{y}_i^2 \tag{6}$$

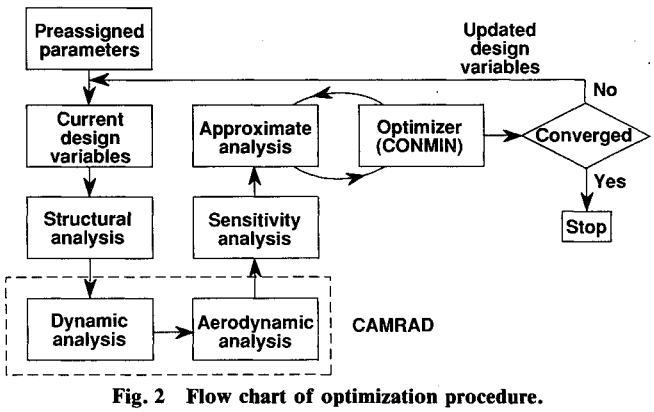

Fig. 2 Flow chart of optimization procedure.

The centrifugal stress in the ith segment is calculated as follows:

$$\sigma_i = \frac{\sum_{j=i}^{\text{NSEG}} W_j \Omega^2 \hat{y}_j}{A_i} \tag{7}$$

Analysis

The optimization procedure with integrated aerodynamics and dynamics is described next. The procedure uses the Comprehensive Analytical Model of Rotorcraft Aerodynamics and Dynamics[22] (CAMRAD) analysis to model both blade aerodynamics and dynamics. The basic algorithm used for optimization is the method of feasible directions implemented in the program CONMIN[23] along with an approximate analysis.

Aerodynamic Analysis

CAMRAD is used to calculate the section loading from the airfoil two-dimensional aerodynamic characteristics. It uses the lifting line or blade element approach and has corrections for yawed and three-dimensional flow effects.[24] The code is run using the following assumptions: uniform inflow, yawed flow on the rotor, unsteady aerodynamics, and no dynamic stall. It offers two broad categories of trimming – free flight and wind tunnel. The wind-tunnel trim option is used herein since a wind-tunnel model rotor is considered. The trim option consists of trimming the rotor lift and drag, each normalized by solidity and the flapping angle with collective pitch, cyclic pitch, and shaft angle. The blade is trimmed for the specified flight condition at each step of design optimization.

Dynamic Analysis

In CAMRAD, the blade response is computed using rotating free-vibration modes, equivalent to a Galerkin analysis.[24] Ten bending modes are calculated, of which seven are flapping (one rigid and six elastic), three lead-lag (one rigid and two elastic) and one is a rigid-body torsion mode. Main blade responses up to 8/rev are included. Therefore, eight harmonics of the rotor revolution are retained in the air loads calculation. The 4/rev vertical shear is calculated using the airloads information obtained from the aerodynamic analysis.

Optimization Implementation

The optimization procedure is shown in Fig. 2. The process is initiated by identifying the blade preassigned parameters which are held fixed during optimization. The next step is to initialize the design variables and to perform the blade structural analysis to calculate blade properties such as centrifugal stress and autorotational inertia. The aerodynamic and dynamic analyses are performed next using CAMRAD. The sensitivity analysis consists of evaluations of the derivatives of the objective function and the constraints with respect to the design variables. Analytical derivatives are used for the weight, autorotational inertia, and centrifugal stress. Forward finite differences are used for the derivatives of the hub shear and the frequencies. Once the sensitivity analysis is completed, optimization is performed.

The optimization process requires many evaluations of the objective functions and constraints before an optimum design is obtained. Therefore, an approximate analysis is used along with CONMIN to save computational effort. In the present work, the objective function and constraints are approximated by linear Taylor series expansions. The expansions provide the changes in the objective functions and constraints in terms of the derivatives and changes in the design variables. The assumption of linearity is valid over small increments in the design variable values and does not introduce large errors if the increments are small. Move limits, defined as the maximum fractional change of each design variable value, are imposed as upper and lower bounds on each design variable. Using CON-

MIN, along with the approximate analysis, updated design variable values are obtained. The process continues until convergence is achieved. A full cycle comprises CAMRAD, sensitivity analysis, and optimization. Convergence is checked on the objective function value over three consecutive cycles using a tolerance of 0.5×10^{-5}.

Test Problem

The baseline blade model selected is a version of an advanced wind tunnel model of the Growth Black Hawk[25] type. It is an articulated four-bladed rotor with a rigid hub. It has a rectangular planform, a linear twist distribution, and a single airfoil throughout the span. Eight structural nodes and 14 aerodynamic segments are used to model the blade in CAMRAD. Table 2 contains the parameters of the baseline or the "reference" rotor which are fixed during design optimization. The values of the first four rotating elastic natural frequencies of the blade, which are constrained during optimization, along with the prescribed bounds, are listed in Table 3. The blade is optimized for a forward flight condition with an advance ratio of $\mu = 0.30$. A minimum value α of 19.748 lb-ft^2 is used for the autorotational inertia constraint. An allowable stress σ_{max} of 2×10^7 lb/ft^2 and factor of safety $FS = 2$ are used for the centrifugal stress constraint.

Results and Discussion

This section of the paper presents results from the three formulations summarized in Table 1. Results for each of the three problem formulations are presented in Table 4. Column 1 presents the reference blade data, and columns 2–4 present the corresponding information for the optimum blades. In the formulations presented here, optimum results have been obtained within 7–10 cycles. In the following discussions, the effect of optimization on blade dynamics is assessed by studying the nature of the first four elastic modes associated with the frequencies f_3–f_6 constrained during optimization. The effect of optimization on air load distributions is discussed and the total power required by the rotor investigated. In all of the optimization results obtained, stability is assured since the center of mass of the blade remained forward of the quarter chord point. This is due to the variations of the stiffnesses assumed along the blade radius, which do not allow large perturbations of the center of mass.

Weight Minimization (Formulation 1)

The design obtained using blade weight as the single objective function is presented in column 2 of Table 4 and in Figs. 3 and 4. After optimization, the natural frequency of the fourth elastic mode f_6 is at its prescribed upper bound, and the autorotational inertia constraint is at its prescribed lower bound. The optimum blade has a taper ratio of 1.17, and the values of the stiffnesses EI_{xx_r} and EI_{zz_r} are increased from their corresponding reference blade values. However, the value of the torsional stiffness at the blade root GJ_r remains unchanged after optimization since no constraints are imposed on the blade torsional frequencies. The values of the design variables k_r and c_r are also reduced after optimization. The reduced root chord c_r and the increased taper ratio λ result in a 19.7% reduction in the blade solidity as shown in Table 4. The nonstructural masses are also reduced significantly as shown in Fig. 3. Figure 4a indicates that the blade weight, which is the objective function, reduces (by 7.5%) from the corresponding reference blade value. It is interesting to note from Fig. 4b that the value of the 4/rev vertical shear is reduced by 40.6% from the reference blade value, although it was not included in this formulation.

Table 2 Test problem parameters

Blade radius	4.685 ft
Number of blades	4
Rotational speed	639.5
Flap hinge offset/radius	0.0534
Inplane hinge offset/radius	0.0534
Maximum twist (at blade tip)	−16 deg
Advance ratio	0.3

Table 3 Blade frequencies (per rev) and bounds (windows)

			Prescribed bounds	
	Mode	Reference	Lower	Upper
f_3	Flapping	3.068	3.05	3.50
f_4	Flapping	6.763	6.50	6.90
f_5	Flapping	9.283	9.25	9.50
f_6	Lead-lag	12.632	12.50	12.75

Vertical Hub Shear Minimization (Formulation 2)

The design with 4/rev vertical hub shear as the single objective function is summarized in column 3 of Table 4 and in Figs. 3 and 4. The third elastic coupled natural frequency f_5 reaches the prescribed lower bound, and the autorotational inertia constraint is again at its prescribed lower bound. The optimum blade is tapered with the taper ratio 1.18. The values of EI_{xx_r} and EI_{zz_r} are higher than their corresponding reference blade values. The value of GJ_r remains unchanged during optimization for the reason described previously. The values of k_r and c_r are once again reduced after optimization resulting in a reduction of the solidity by 41.8%. The nonstructural masses are also reduced significantly as shown in Fig. 3. Figure 4b shows a very significant reduction in the 4/rev vertical hub shear (85.6%), the objective function, from the reference blade value. The total blade weight is reduced, as shown in Fig. 4a (by 8.5%), although it is not used as a design criterion in this formulation. The reduction in blade weight is larger in this formulation than in the preceding formulation where the blade weight is the objective function. This points to the fact that the optimum weight obtained from formulation 1 is possibly a local minimum.

Combined Weight and Hub Shear Minimization (Formulation 3)

Even though formulation 1 (and possibly formulation 2) reached local minimum, the values obtained from these individual optimizations are lower than the reference blade values

Table 4 Optimization results

		Formulation		
	Reference	1	2	3
EI_{xx_r}, lb-ft^2	10,277	11,305	10,306	11,818
EI_{zz_r}, lb-ft^2	354	389	385	402
GJ_r, lb-ft^2	261	261	261	261
k_r, ft	0.268	0.192	0.175	0.176
λ	1.000	1.170	1.180	1.33
c_r, ft	0.450	0.403	0.295	0.28
f_3, per rev	3.068	3.194	3.271	3.282
f_4, per rev	6.763	6.853	6.870	6.815
f_5, per rev	9.283	9.415	9.250	9.487
f_6, per rev	12.632	12.750	12.749	12.512
AI, lb-ft^2	19.75	19.75	19.75	19.96
4/rev hub shear, lb	0.160	0.095	0.023	0.036
Percent reduction in 4/rev hub shear	—	40.61	85.6	77.6
Blade weight, lb	3.408	3.152	3.120	3.048
Percent reduction in blade weight	—	7.51	8.5	10.6
C_p/s	0.004	0.0039	0.0037	0.036
Percent reduction in C_p/s	—	4.3	8.5	9.6
Blade solidity, s	0.122	0.098	0.071	0.062

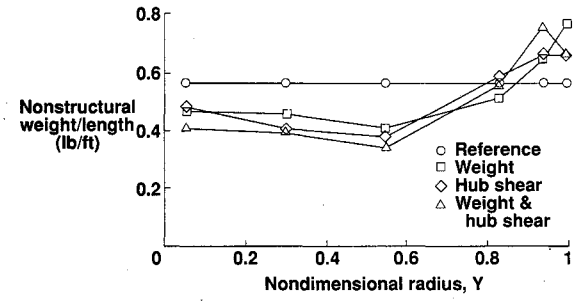

Fig. 3 Nonstructural weight distributions.

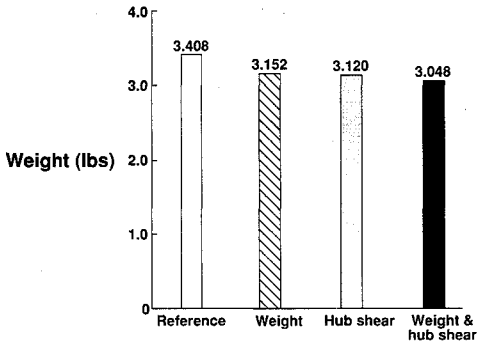

a) Blade weight

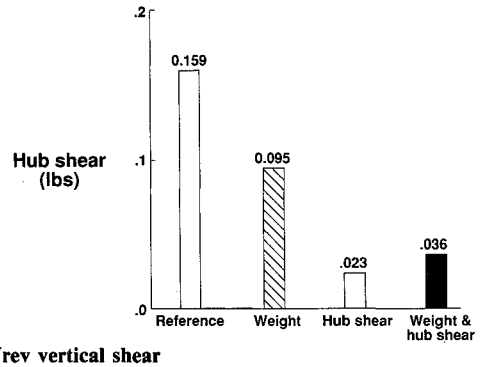

b) 4/rev vertical shear

Fig. 4 Comparison of optimum weight and hub shear.

and, therefore, still serve as useful targets in the Global Criteria Approach. Results of the simultaneous minimization of the blade weight and hub shear are summarized in column 4 of Table 4 and in Figs. 3 and 4 The constraints are all satisfied and the autorotational inertia constraint is greater than its prescribed lower bound. The optimum blade has a taper ratio of 1.33, which is larger than in the other formulations. The optimum values of the bending stiffnesses EI_{xx_r} and EI_{zz_r} are higher than their respective reference blade values and the value of the torsional stiffness GJ_r remains unaltered. The reductions in the value of c_r and therefore in the value of blade solidity are the largest at 37.5 and 49.2%, respectively. The 4/rev vertical hub shear is reduced by 77.6% and the blade weight by 10.6% (Figs. 3 and 4).

Additional Comparisons of Designs

The distributions of the nonstructural weight/unit length for all three formulations, before and after optimization, are shown in Fig. 3. In all formulations the nonstructural weight increases outboard after optimization due to the presence of the autorotational inertia constraint. The trend is more significant in formulation 2 (vertical hub shear) than in formulation 1 (weight) and is most significant in formulation 3 (weight and hub shear). It is interesting to note that in the hub shear and the multiple objective function formulations, the maximum

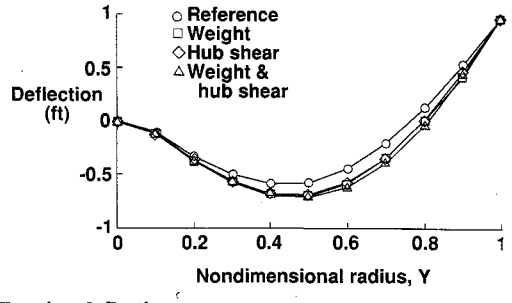

a) Flapping deflections

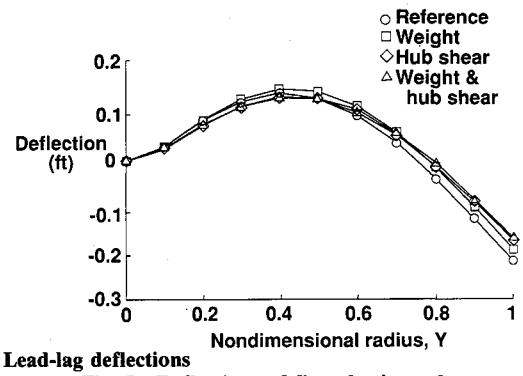

b) Lead-lag deflections

Fig. 5 Deflections of first elastic mode.

values of nonstructural weights occur at the next to last node and not at the last node as in the weight optimization formulation. This could be due to some changes in the coupled mode shapes affected by modified stiffness distributions when the hub shear is minimized either separately or simultaneously with the weight. Figure 4 presents comparisons of optimum weight (Fig. 4a) and vertical hub shear (Fig. 4b) from all three formulations. As shown in Fig. 4 and Table 4, the Global Criteria Approach provides the lightest blade structure with a hub shear reduction that falls between those obtained from the single objective function optimizations. This is contrary to the intuitive belief that the use of a multiple objective formulation should yield solutions lying between those of the single objective formulations. In other words, the blade weight obtained by simultaneously minimizing weight and hub shear might be expected to be higher than that obtained from weight minimization, and the hub shear obtained should be higher than that obtained from hub shear minimization. However, this is only true if the individual optimizations (formulations 1 and 2) each obtain a global minimum. For the purpose of this work, the interest was mainly to obtain improved values of $W(\phi_1^*)$ and $F_z(\phi_2^*)$, even if they are not global minima.

Effect of Optimization on Mode Shapes

There was an interest in addressing the effect of optimization on the mode shapes associated with the frequencies constrained during the optimization procedure. Therefore, the mode shapes for the first four elastic modes are plotted before and after optimization in Figs. 5–8, respectively. Part (a) of each figure shows the flapping components, and part (b) shows the lead-lag components of the coupled modes. In each of these figures, the deflections are based on taking the tip deflection to be one. The figures indicate that there is a change in the magnitude of the modal deflections after optimization and, in most cases, the node points of the modal deflections are moved slightly outboard from the reference blade. However, no major changes in the nature of the mode shapes occur.

Effect of Optimization on Blade Aerodynamics

Effect on Air Loads

Reduction of vertical hub shear is achieved when any of the following occurs: blade natural frequencies move away from

the excitation frequencies; mode shapes become more nearly orthogonal to the forcing function, or blade harmonic air loads are reduced. It was of interest in the present work to investigate the extent to which the optimization process alters the distribution of air loads.

The influence of the design variables on the section aerodynamic load normal to the plane of the rotor F_p is assessed by comparing its radial and azimuthal distributions before and after optimization. Figure 9 presents the radial distributions of F_p for the advancing blade at $\Psi_i = 90$ deg, for both the reference and the optimum blades. Note that the high negative value of F_p near the tip is caused by the high negative twist of 16 deg (Table 2) in which the tip of the blade has a smaller pitch angle than the root. Blades with negative twist may carry negative lift outboard and positive lift inboard on the advancing side. Figure 9 indicates that the optimum rotor has lower vertical air load throughout the span. The reduction is largest in formulation 3.

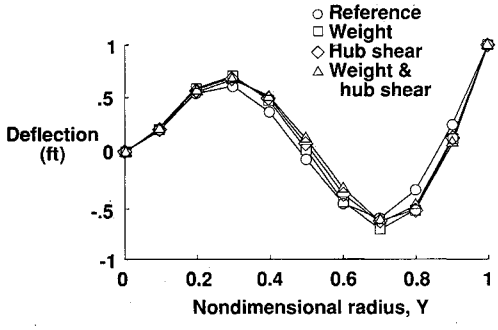

a) Flapping deflections

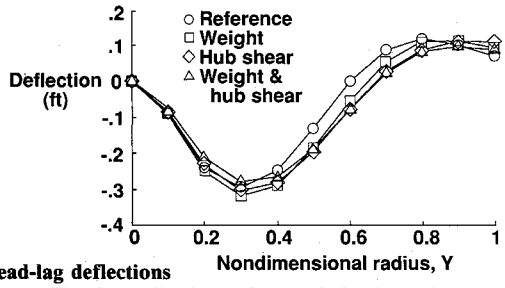

b) Lead-lag deflections

Fig. 6 Deflections of second elastic mode.

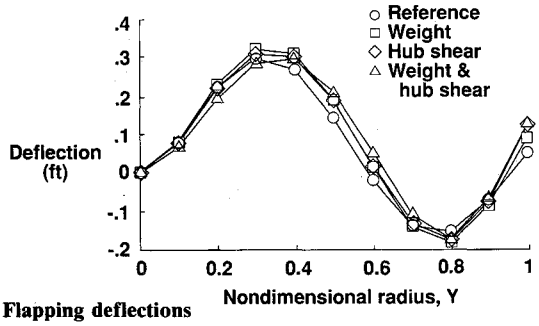

a) Flapping deflections

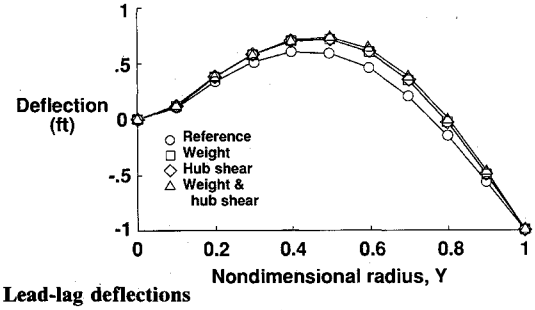

b) Lead-lag deflections

Fig. 7 Deflections of third elastic mode.

In Figs. 10–12, the azimuthal distributions of the vertical air load F_p are plotted for three radial locations: near the blade root (Fig. 10, $Y = 0.25$), at the point of thrust-weighted equivalent chord (Fig. 11, $Y = 0.75$), and near the blade tip (Fig. 12, $Y = 0.99$). These figures also indicate that the optimum rotor has lower values of the amplitudes of the azimuthal distributions of the vertical air load. Further, formulation 3 produces the maximum reductions. The reason for the air load reductions can be explained as follows. The optimum rotor was required to maintain the same C_T/s as the reference rotor; therefore, since during optimization the solidity of the optimum rotor reduces significantly, the thrust carried by the optimum rotor has to reduce. This is reflected through the reduction of F_p in Figs. 9–12. The reductions are most significant in formulation 3 due to the maximum reduction in s (49.2%) in this case. Therefore, to make a more meaningful comparison, F_p/s is plotted in Fig. 13 to study the effect of optimization on the vertical blade loading for a given area. Figure 13 shows that all of the four blades (reference and the three optimum) produce about the same integrated vertical force per unit area over the blade span. In fact, the optimum blades have somewhat higher values, indicating that at any radial location the optimum blades use the area more effectively. The best results are obtained using formulation 3.

Effect on Power Required

Finally, the total power required by the rotor to provide the same amount of thrust is checked before and after optimization. Recalling the fact that the solidity of the optimum rotor is much smaller compared to the reference rotor, the nondimensional power coefficient C_p is normalized with s and is presented in Table 4. Table 4 indicates that the total power

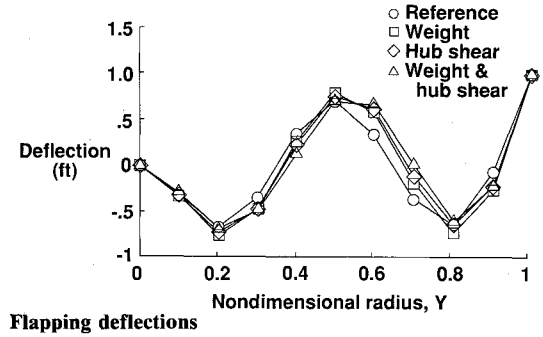

a) Flapping deflections

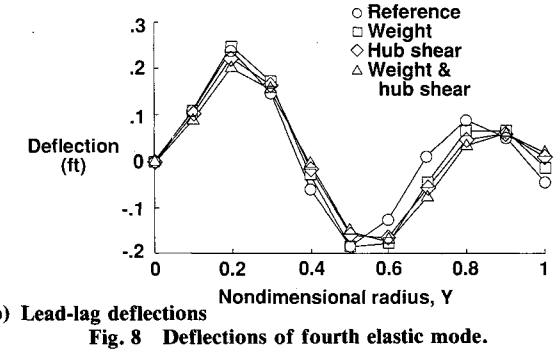

b) Lead-lag deflections

Fig. 8 Deflections of fourth elastic mode.

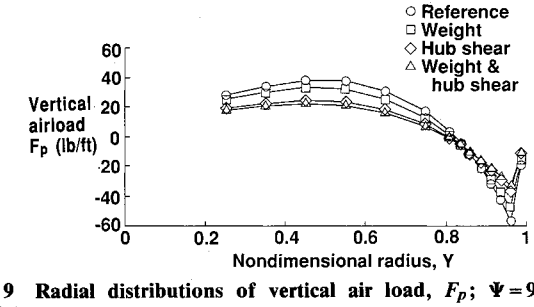

Fig. 9 Radial distributions of vertical air load, F_p; $\Psi = 90$ deg, $\mu = 0.3$.

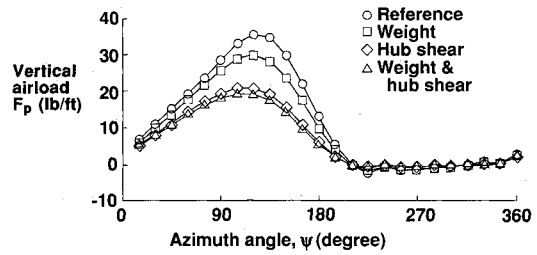

Fig. 10 Azimuthal distributions of vertical air load, F_p; $Y = 0.25$, $\mu = 0.3$.

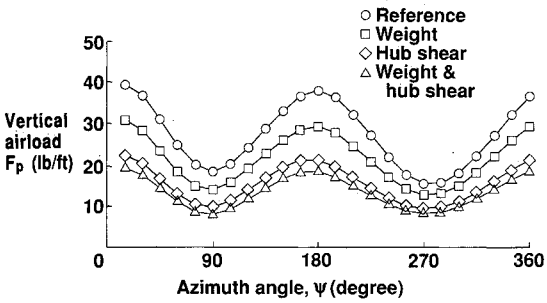

Fig. 11 Azimuthal distributions of vertical air load, F_p; $Y = 0.75$, $\mu = 0.3$.

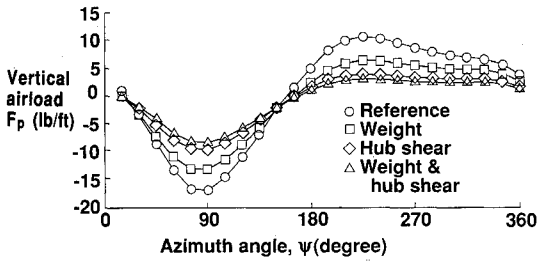

Fig. 12 Azimuthal distributions of vertical air load, F_p; $Y = 0.99$, $\mu = 0.3$.

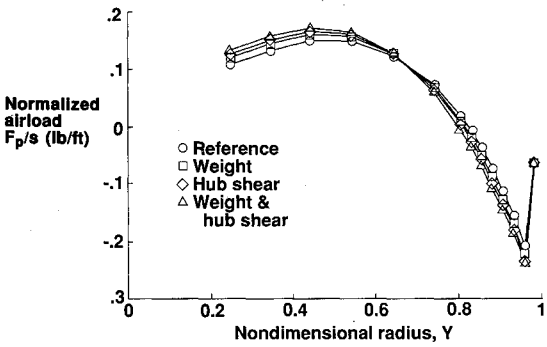

Fig. 13 Radial distributions of normalized vertical air load, F_p/s; $\Psi = 90$ deg, $\mu = 0.3$.

required to produce the same amount of thrust for a given area reduces significantly after optimization and that the reduction is most significant in formulation 3. Hence, optimization not only improves the net rotor power requirement, which should reduce since the solidity of the blade is reduced, but also reduces the power per unit area.

Concluding Remarks

In this paper, rotor blade designs are generated by use of an integrated aerodynamic load/dynamic optimization procedure. Blade weight and 4/rev vertical hub shear are minimized in the presence of air loads, under forward flight conditions, using both single and multiple objective functions formulations. Constraints are imposed on the first four elastic coupled natural frequencies, the blade autorotational inertia, and the centrifugal stress. The program CAMRAD is used for the blade dynamic and aerodynamic analyses, and the program CONMIN along with an approximate analysis procedure is used for optimization. The Global Criteria Approach is used for the multiple objective formulation, and its results are compared with those obtained from single objective function formulations. The optimum designs are compared with those of a reference blade. The optimization scheme used is very efficient, typically requiring 7-10 cycles to converge. The following observations are made from this study.

1) The Global Criteria Approach for formulating the multiple objective function optimization was very effective. The approach yielded a design in which the blade weight and vertical hub shear were significantly reduced relative to the reference blade.

2) The optimum blades were all tapered in contrast to the reference blade, which was rectangular. In all three optimization formulations studied, stability was assured since the center of mass of the blade remained forward of the quarter chord due to the design variables used.

3) Inspection of the vertical air load distributions for the initial and the optimum designs indicated that optimization significantly reduced the amplitude of this distribution due to reduced thrust requirement. However, the optimum rotors maintained slightly higher values of the vertical force per unit area, indicating a more effective use of the area.

4) The optimization procedure changed the modal deflections slightly and in most cases moved the node points of the associated modes somewhat outboard, but no significant changes occurred in the nature of the mode shapes.

5) As a result of optimization, the total power required to produce the same amount of thrust for a given area was reduced.

Acknowledgments

The authors gratefully acknowledge the helpful suggestions of Henry Jones, Howard Adelman, J. Sobieski, and Matthew Wilbur.

References

[1]Ashley, H., "On Making Things the Best—Aeronautical Use of Optimization," *Journal of Aircraft*, Vol. 19, No. 1, 1982, pp. 5-28.

[2]Sobieszczanski-Sobieski, J., "Structural Optimization Challenges and Opportunities," *Proceedings of the International Conference on Modern Vehicle Design Analysis*, London, England, June 1983.

[3]Sobieszczanski-Sobieski, J., (ed.), "Recent Experiences in Multidisciplinary Analysis and Optimization, NASA CP-2327, April 1984.

[4]Miura, H., "Application of Numerical Optimization Method to Helicopter Design Problems: A Survey," NASA TM-86010, Oct. 1984.

[5]Bennett, R. L., "Application of Optimization Methods to Rotor Design Problems," *Vertica*, Vol. 7, No. 3, 1983, pp. 201-208.

[6]Celi, R., and Friedmann, P. P., "Efficient Structural Optimization of Rotor Blades with Straight and Swept Tips," *Proceedings of the 13th European Rotorcraft Forum*, Sept. 1987, Paper No. 3-1.

[7]Lim, J. W., and Chopra, I., "Stability Sensitivity Analysis for the Aeroelastic Optimization of a Helicopter Rotor," AIAA Paper 88-2310, April 1988.

[8]Walsh, J. L., Bingham, G. J., and Riley, M. F., "Optimization Methods Applied to the Aerodynamic Design of Helicopter Rotor Blades," *Journal of the American Helicopter Society*, Vol. 32, No. 4, Oct. 1987, pp. 39-44.

[9]Helicopter Engineering, Pt. 1, Preliminary Design, AMCP 706-201, Aug. 1974.

[10]Reichert, G., "Helicopter Vibration Control – A Survey," *Vertica*, Vol. 5, 1981, pp. 1-20.

[11]Taylor, R. B., "Helicopter Vibration Reduction by Rotor Blade Modal Shaping," *Proceedings of the 38th Annual Forum of the American Helicopter Society*, May 1982, pp. 90-101.

[12]Peters, D. A., Ko, T., Korn, A., and Rossow, M. P., "Design of

Helicopter Rotor Blades for Desired Placements of Natural Frequencies," *Proceedings of the 39th Annual Forum of the American Helicopter Society,* May 1983.

[13]Nixon, M. W., "Preliminary Structural Design of Composite Main Rotor Blades for Minimum Weight," NASA TP-2730, July 1987.

[14]Chattopadhyay, A., and Walsh, J. L., "Minimum Weight Design of Rectangular and Tapered Helicopter Rotor Blades with Frequency Constraints," *AHS Journal,* American Helicopter Society, Washington, DC, Vol. 34, No. 4, Oct. 1989, pp. 77–82; NASA TM-100561, Feb. 1988.

[15]Chattopadhyay, A., and Walsh, J. L., "Application of Optimization Methods to Helicopter Rotor Blade Design," AIAA Paper 88-2337-CP, April 1988; also NASA TM-100569, March 1988.

[16]Hanagud, S., Chattopadhyay, A., Yillikci, Y. K., Schrage, D., and Reichert, G., "Optimum Design of a Helicopter Rotor Blade," *Proceedings of the 12th European Rotorcraft Forum,* Sept. 1986, Paper No. 12, Garmisch-Partenkirchen, Germany.

[17]Weller, W. H., and Davis, M. W., "Experimental Verification of Helicopter Blade Designs Optimized for Minimum Vibration," *Proceedings of the 44th Annual Forum of the American Helicopter Society,* June 1988, Washington, DC, pp. 263–279.

[18]Peters, D. A., Rossow, M. P., Korn, A., and Ko, T., "Design of Helicopter Rotor Blades for Optimum Dynamic Characteristics," *Computers & Mathematics with Applications,* Vol. 12A, No. 1, 1986, pp. 85–109.

[19]Chattopadhyay, A., and Walsh, J. L., "Structural Optimization of Rotor Blades with Integrated Dynamics and Aerodynamics," NASA TM-101512, Oct. 1988.

[20]Adelman, H. M., and Mantay, W. R., "An Initiative in Integrated Multidisciplinary Optimization of Rotorcraft," NASA TM-101523, Oct. 1988.

[21]Rao, S. S., "Multiobjective Optimization in Structural Design with Uncertain Parameters and Stochastic Processes" *AIAA Journal,* Vol. 22, No. 11, 1984, pp. 1670–1678.

[22]Johnson, W., "A Comprehensive Analytical Model of Rotorcraft Aerodynamics and Dynamics," *Part II: User's Manual,* NASA TM-81183, June 1980.

[23]Vanderplaats, G. N., "CONMIN – A FORTRAN Program for Constrained Function Minimization," *User's Manual,* NASA TM X-62282, Aug. 1973.

[24]Johnson, W., "A Comprehensive Analytical Model of Rotorcraft Aerodynamics and Dynamics," *Part I: Analysis Development,* NASA TM-81182, June 1980.

[25]Yeager, W., Mantay, W., Wilbur, M., Cramer, R., and Singleton, J., "Wind Tunnel Evaluation of an Advanced Main Rotor Blade Design for a Utility Class Helicopter," NASA TM-89129, Sept. 1987.

[26]Chattopadhyay, A., Walsh, J. L., and Riley, M. F., "Integrated Aerodynamic/Dynamic Optimization of Helicopter Rotor Blades, NASA TM-101553, Feb. 1989.